Published in final edited form as:

Curr Opin Neurobiol. 2004 October ; 14(5): 617–628. doi:10.1016/j.conb.2004.08.017.

Fiber optic *in vivo* imaging in the mammalian nervous system

Amit D Mehta[1,2], **Juergen C Jung**[1,2,3], **Benjamin A Flusberg**[2], and **Mark J Schnitzer**[1,2,*]

[1]Department of Biological Sciences, Stanford University, Stanford, CA 94305, USA

[2]Department of Applied Physics, Stanford University, Stanford, CA 94305, USA

[3]Department of Pharmacology, Oxford University, Oxford, OX1 3QT, United Kingdom

Abstract

The compact size, mechanical flexibility, and growing functionality of optical fiber and fiber optic devices are enabling several new modalities for imaging the mammalian nervous system *in vivo*. Fluorescence microendoscopy is a minimally invasive fiber modality that provides cellular resolution in deep brain areas. Diffuse optical tomography is a non-invasive modality that uses assemblies of fiber optic emitters and detectors on the cranium for volumetric imaging of brain activation. Optical coherence tomography is a sensitive interferometric imaging technique that can be implemented in a variety of fiber based formats and that might allow intrinsic optical detection of brain activity at a high resolution. Miniaturized fiber optic microscopy permits cellular level imaging in the brains of behaving animals. Together, these modalities will enable new uses of imaging in the intact nervous system for both research and clinical applications.

Introduction

The development of new optical imaging techniques in the past decade has greatly increased the range of issues in mammalian neurobiology that can be addressed using light. Although most optical studies have been performed *in vitro*, fiber optic approaches are expanding the applicability of optical methods to live mammals. Here, we review the general advantages of fiber optic imaging, recent progress in the application of several fluorescence and intrinsic signal fiber optic modalities in neurobiology, and advances towards fiber optic imaging in behaving animals.

A conventional optical fiber channels light between distal locations by total internal reflection [1], which permits light propagation in one or more optical modes within an inner core of the fiber that has a slightly higher index of refraction than the surrounding cladding zone. Fibers commonly range from about 80 μm to several millimeters in diameter and are typically made from glass or plastic. Use of optical fibers for *in vivo* imaging offers key mechanical benefits regarding device size and flexibility, as well as advantages concerning the performance and availability of fiber optic components, as discussed below.

Mechanical flexibility: depending on its diameter and composition, an optical fiber can be bent without mechanical damage with a minimal turning radius that generally varies from around one millimeter to several tens of centimeters. This flexibility can be harnessed to access tissues through circuitous routes or to image within freely moving subjects.

*mschnitz@stanford.edu.

Edited by Winfried Denk and Liqun Luo

Compact size: the small diameter of many fiber types allows the construction of minimally invasive endoscopes that can be inserted into the body, as well as the large-scale assembly of many optical fibers on the cranium for non-invasive optical studies.

Quality optical components: there have been significant recent advances in the miniaturization of fiber optic devices, as well as in the range and performance of their optical functions. When available, comparable devices that manipulate light traveling through free space are typically much bulkier than their fiber optic counterparts. Particularly in the case of infrared wavelengths used as telecom standards, fiber devices often provide performance that is comparable or superior to free-space versions but with reduced need for time-consuming optical alignments.

Several fluorescence and intrinsic optical imaging modalities exploit these benefits of optical fibers and produce images using a few common fiber arrangements (Table 1). Light from a single fiber can be scanned across tissue while a pictorial representation is constructed pixel by pixel. Alternatively, multiple fibers can carry light to or from distinct sample locations, which can be monitored concurrently or in succession to create an image. Large ordered arrays of fibers can transmit entire images of up to ~100 000 pixels, with each fiber in the array carrying light for a single pixel.

Fluorescence microendoscopy

Although two-photon fluorescence microscopy provides typical penetration depths of up to~600 μm within tissue [2,3], the majority of the mammalian brain has remained outside the reach of *in vivo* microscopy. The recent development of submillimeter-diameter endoscopes, or 'microendoscopes', that exhibit micron-scale resolution [4•,5••,6••,7,8] has allowed *in vivo* cellular level imaging within deep brain tissues previously inaccessible to microscopy [5••,6••]. Microendoscopes that can be inserted into tissue in a minimally invasive manner have been explored previously for ophthalmic and otological applications, but these devices were often broader than 1 mm in diameter and could not resolve individual cells [9,10]. Fiber optic confocal fluorescence endoscopes that exhibit 1–8 mm diameters [11–13] have generally been too large for insertion directly into brain tissue. The use of epi-fluorescence endoscopes for voltage-sensitive dye imaging of brain activity has been limited to the neocortical surface [14]. Recent devices for high-resolution fluorescence microendoscopy (FME) range from 350 to 1000 μm in diameter and are based on one or more microlenses of the gradient refractive index (GRIN) variety with numerical apertures of up to 0.5–0.6 (Figure 1a; [4•,5••,6••,13]).

Cylindrically shaped GRIN lenses act like optical fibers in the sense that they transmit light between distal locations using total internal reflection. In these lenses, the refractive index declines gradually from its highest value on the cylindrical axis to values 1–6% lower at the radial periphery (e.g. [15]). Unlike with fibers that exhibit a discrete difference in index between core and cladding, the graded index profile reduces dispersion between spatial modes [1] and permits a GRIN microendoscope to project a real image of the specimen without using a fiber bundle array (Figure 1b; [5••]). The lack of pixilation helps to achieve image resolution as good as ~0.9 μm [5••,6••]. One-photon epi-fluorescence imaging using FME (Figure 1b) has enabled visualization of individual neurons and provided video-rate movies of red blood cell dynamics within deep areas of the rodent brain (Figure 1c,d; [5••]). Although this modality offers fast frame-rate acquisition, it lacks optical sectioning. Two-photon fluorescence microendoscopy (2PFME) is a laser-scanning imaging modality that provides similar depth penetration, robustness to light scattering, and inherent optical sectioning as two-photon microscopy, but using a minimally invasive probe (Figure 1e,f; [4•,5••,6••,8]). These capabilities have enabled visualization by 2PFME of fluorescent layer V pyramidal cells [6••] and hippocampal pyramidal cell bodies and dendrites [5••] up to nearly 300 μm from the microendoscope probe in anesthetized mice (Figure 1f; [5••]). Confocal FME that combines

micro-lenses with a fiber bundle provides a flexible hand-held probe, but in doing so sacrifices focusing ability [7,13]. Pixilation of the image in the bundle also degrades resolution to the 2–5 μm scale [7,11–13].

Although FME remains in infancy, it seems well poised to achieve widespread application because of its ability to provide high-resolution *in vivo* imaging of deep brain areas. However, demonstration of 800–1000 μm imaging depths using two-photon microscopy with a regenerative amplifier light source [16•,17], and development of surgical tactics that allow visualization, albeit somewhat invasive, of dorsal hippocampal tissue by conventional microscopy [18•] might lead to alternatives for high-resolution imaging in certain brain areas. An outstanding issue for FME concerns the degree of tissue damage accompanying probe insertion [5••,6••]. Further studies must address this issue carefully, and optimal insertion methods, perhaps involving cannulation, need to be developed. Other likely advances include improved resolution for visualizing fine cellular structures, development of chronic imaging preparations, and creation of FME devices for use in freely moving animals.

Imaging of intrinsic optical signals

Several fiber optic modalities are being developed to exploit the intrinsic optical properties of brain tissue and optical correlates of brain activity that have traditionally been studied without fibers (Table 1). Metabolic responses to brain activity that can be detected optically include changes in blood flow [19,20], hemoglobin oxygenation [20–22], oxygen tension [23], and redox states of intracellular NADH [24,25] and flavoproteins [26,27]. Such effects generally occur within 0.1–60 s of neural activation and cause changes in mean absorption [22,28] or auto-fluorescence [24–26,29] of about 0.1–4% that have been widely used for functional mapping [26,30,31]. Faster effects that may arise more directly from neuronal depolarization than from metabolism involve changes in neuronal volume or refractive index and occur within ~1 ms or less of neural activation. These faster phenomena alter light scattering by 0.0001–0.01% [32,33] and remain poorly understood and hard to detect. Fiber optics are being harnessed to examine both slow and fast signals *in vivo*.

Diffuse optical imaging and tomography

Researchers are increasingly performing near infrared absorption spectroscopy (NIRS) studies of brain activation using assemblies of fiber optic emitters and detectors, typically spaced about 5–40 mm apart on the head, to deliver and collect light through the intact skull (Figure 2a,d; [34–40]). Because scattering lengths of near infrared light in the brain are at most hundreds of microns but absorption lengths are in the millimeter to centimeter range, photons undergo multiple scattering events and migrate diffusively between emitters and detectors. This enables diffuse optical imaging (DOI), in which changes in optical fluence between pairs of emitter and detector fibers (Figure 2) are usually ascribed to changes in light absorption within tissue. The inverse problem of taking these measured pairwise changes in fluence and working backwards to reconstruct the spatiotemporal images of absorption changes within tissue is usually mathematically underdetermined and complicated by cardiac and respiratory artifacts. Ongoing improvement of heuristics for image reconstruction and for artifact removal continues to be key to the development of DOI.

Most DOI studies of the brain examine slow absorption changes arising from activity-dependent variations in blood flow and hemoglobin oxygenation. In rat [41] and human subjects [42•], the temporal resolution of NIRS is similar to that of functional magnetic resonance imaging (fMRI), which also relies on hemodynamic effects (Figure 2e). However, use of two or more wavelengths for NIRS permits changes in total blood content and in both oxy- and deoxy-hemoglobin concentrations to be distinguished, which conventional fMRI does not allow. A few groups have explored fast changes in optical fluence occurring <100 ms

following sensory stimulation, effects believed to arise from changes in light scattering on the basis of their rapidity [43–45]. Although diffuse photon migration limits the penetration depth and spatial resolution of DOI to the centimeter-scale in humans, such non-invasive measurements provide a low-cost means of identifying regions of brain activation [46], for example with subjects who cannot undergo MRI [35,37,47]. Commercial DOI systems for use in humans are already available.

Diffuse optical tomography (DOT) is a form of DOI that can provide volumetric information by seeking an optimal solution to the image reconstruction problem [34,41,48••,49], rather than the two-dimensional images commonly obtained by interpolation between fibers [39,46, 47]. A key facet of DOT is that each detector should receive light from emitters beyond its nearest neighbors. Such 'overlapping' measurements enable volumetric imaging and resolution that is superior to the distance between fibers [38,40,48••]. Issues concerning the limits to spatial resolution with DOT are complex, because fiber array geometry [50,51], cranial shape [52,53], depth below the scalp, and uncertainties in fiber location [48••] and orientation [40, 54,55] all influence resolution. In small animals, in which the distance from scalp to cortex is short, close packing of fibers yields superior resolution than can be obtained in adult humans, for which the skull thickness is a key limitation. Activated areas of the rodent brain may be similarly identified by DOT and fMRI, as demonstrated using rat forepaw stimulation (Figure 2c; [48••]). Thus, a broadly applicable advance that appears within reach is development of DOT for use in freely behaving animals. Other advances might come from improved analysis of blood chromophore concentrations [56,57], optical assemblies that can incorporate large numbers of precisely oriented channels using a non-contact mode displaced from tissue [54, 55], and improved algorithms for reducing physiological noise artifacts [38,58]. Eventually, dense arrays of integrated semiconductor emitters and photodetectors [59] might obviate the need for optical fibers and significantly enhance resolution.

Optical coherence tomography

Optical coherence tomography (OCT) uses light that is backscattered off tissue to provide image contrast. Analogous to forms of ultrasound imaging, OCT offers inherent optical sectioning by tracking photons' round-trip time of flight from source to tissue and back to detector. Because the slight differences in travel times from different points in tissue are too short to measure directly, low coherence interferometry (LCI) is used to compare the optical path lengths of light from the sample and the interferometer reference arm (Figure 3a; [60, 61]). Although diffraction determines the lateral resolution of OCT, the coherence length of the optical source, which is inversely related to the spectral bandwidth, determines the axial resolution of optical sectioning. Depending on the wavelength, sources with spectral bandwidths of 50–260 nm can provide axial resolutions as good as 1–14 μm [61,62,63•]. Although it is not strictly necessary to implement OCT within fiber optic hardware [64], this is most commonly done because of the benefits regarding instrument portability, ability to fabricate miniaturized OCT probes [65–68], and availability of superior fiber optic components for telecom wavelengths, such as 850 and 1310 nm.

Despite ambiguities in image interpretation that can arise from confounds between absorption and scattering (Figure 3) and from uncertainty in the biological features that scatter light, OCT has found increasing application for *in vivo* imaging of tissue laminae (e.g. [61,62,63•,65]). Some large cell types are also discernible, for example in *Xenopus laevis* tadpoles [61,63•, 69–71] and in meningiomas [64]. The best developed application is visualization of the human retina, which has been accomplished *in vivo* with 'ultrahigh' resolution of 2–3 μm in the axial dimension (Figure 3; [62,63•]). In the past year, fast spectral detection methods [72•,73,74•] have enabled imaging of the human retina [75–77] and retinal blood flow [78••,79] at up to video-rates (Figure 3d), most recently with ultrahigh resolution [80–82]. OCT measurements

within individual vessels of retinal or brain blood flow responses to neural activation might soon be demonstrated.

A major advantage of OCT is its sensitivity, which can reach the physical limit set by photon shot noise [1], typically −90 to −110 dB relative to the signal from an ideal reflector [60,61], and potentially −120 dB using frequency-swept sources [83,84]. Such high sensitivity has enabled penetration depths of around 500–1000 μm in mammalian brain tissue [85•,86] and up to 2–3 mm in other tissues [61,65]. Although the sensitivity is often mislabeled as the OCT signal to noise ratio, the signal to noise ratio is much lower than ~100 dB because of optical speckle, which arises from interferometric recombination of photons scattered from tissue locations within a coherence length of one another [87]. Speckle creates a multiplicative noise with a mean power proportional to signal power, often 1–10% of signal power across the dynamic range [88].

Because the fractional changes in reflectivity occurring during neural activity are only 0.001–1%, speckle poses a serious obstacle to detection of brain activity by functional optical coherence tomography (fOCT) [85•,89,90•]. Initial fOCT studies of slow intrinsic signals of brain activity in the visual cortex of anesthetized cats found a weak depth dependence to visually driven activity [85•]. It has also been claimed that slow changes in scattering can be detected by fOCT in an *in vitro* preparation of *Aplysia* abdominal ganglion [89]. Measurements in crayfish leg nerve bundles using a differential phase version of LCI for detecting fine displacements revealed fast axonal movements of <1 nm accompanying electrically stimulated action potentials [90•]. These fOCT studies involved either prolonged stimulation over minutes [89] or signal averaging over tens [85•] to hundreds [90•] of stimulation trials. New approaches for reducing speckle [87,91,92] might improve the ability to detect neural activity, but development of an OCT contrast agent [93,94•–96•] that is sensitive to neural activity might be more fruitful.

Spectroscopic information contained in the wavelengths of backscattered light [71,97] may also be useful for examining hemodynamic processes that correlate with neural activation. New broadband sources for ultrahigh-resolution [63•,64,98–102] and spectral detection approaches to high-speed OCT [72•,74–77,78••,79–81] enhance the potential for spectroscopic analysis. Although initial demonstrations of spectroscopic OCT involved broad wavelength bands [71], a pump-probe method for transiently modifying the absorption of a particular molecular species, which can then be detected by LCI, might eventually lead to *in vivo* OCT studies of biochemistry [94•,95•]. Novel contrast mechanisms for OCT that involve harmonic generation or coherent anti-Stokes Raman scattering might also provide specific biological information [103,104].

Fiber optic imaging in freely moving animals

Although electrophysiological and microdialysis studies in behaving mammals are common, optical studies in either restrained alert [21,105–107] or freely moving animals [108–110] remain challenging. Early studies that employed freely moving cats and image-transmitting fiber bundles inserted directly into the brain revealed mainly gross changes in tissue reflectance that correlated with behavioral state [108–110]. Recent studies in restrained alert rats employed a flexible endoscope to acquire intrinsic images, obtained through a thinned skull, of brain activation in response to whisker stimulation [105]. As fiber optic fluorescence methods develop it will be possible to visualize individual neurons in freely moving preparations using a miniaturized optical probe attached to the cranium. However, there are several engineering hurdles involved in this pursuit.

First, the optical probe must be sufficiently small to be borne by a freely behaving animal. Second, the device should retain much of the functionality and imaging quality of conventional

fluorescence microscopy. Third, imaging must be reasonably robust to voluntary and involuntary tissue movements that could cause motion artifacts. Imaging the dynamics of individual neurons in freely moving animals with a probe exhibiting all three characteristics has remained elusive, but work towards attaining this goal took a big step forward with the introduction of a fiber optic miniature two-photon fluorescence microscope that could be mounted on the head of an adult rat [111].

Although slightly bigger (25 g, 1.3 cm diameter, 11 cm tall) than desirable for many behavioral studies, this miniature microscope employed a resonant fiber scanner introduced previously for fiber optic confocal microscopy [112] and succeeded in visualizing neocortical capillaries in freely moving rats, as well as neurons, dendritic spines, and dendritic calcium transients in anesthetized rats [111]. The ultra-short pulses of >1 nJ used for two-photon excitation degrade within conventional single mode fiber because of non-linear optical effects [4•,111], but specialized fibers for ultra-short pulse delivery should obviate this difficulty [113]. Subsequent size reductions of the microscope are preliminary but appear highly promising [114]. For further reductions, micro-machined scanning elements like those used for miniaturized confocal [115,116] and OCT [117–119] imaging should be applicable.

Perhaps the biggest challenge concerns motion artifacts. In freely moving rats, longer periods of useful two-photon imaging were interrupted by intermittent periods of image destabilization [111]. In principle, lateral image motions can be corrected in software using image registration methods, but axial image motions that take a specimen out of focus are more troublesome. Maintaining image clarity will require either active auto-focusing or improved methodologies for reducing tissue motion.

Conclusions

FME, DOT, and OCT are gaining utility for *in vivo* imaging studies of the mammalian nervous system. The use of minimally invasive FME will allow cellular properties to be studied in live animals within deep brain tissues that have been inaccessible to *in vivo* microscopy. DOT and OCT should help increase understanding of the hemodynamic responses to brain activation, and the latter technique should allow studies of such responses within individual blood vessels. For functional brain mapping, these two techniques appear complementary, in that DOT may be better suited for coarser functional mapping studies over broader regions, whereas OCT might enable finer depth-resolved mapping studies over smaller brain regions. In upcoming years, further development of DOT, FME, and miniature fiber optic fluorescence microscopy will enable new studies of brain activity in freely moving animals. When combined with the use of fluorescent indicators of neuronal activity, the latter two methods should permit imaging of cellular dynamics in awake behaving preparations.

Abbreviations

2PFME	two-photon fluorescence microendoscopy
DOI	diffuse optical imaging
DOT	diffuse optical tomography
FME	fluorescence microendoscopy
fMRI	functional magnetic resonance imaging
fOCT	functional optical coherence tomography
GRIN	gradient refractive index
LCI	low coherence interferometry

NIRS	near infrared spectroscopy
OCT	optical coherence tomography

Acknowledgments

MJ Schnitzer is supported by National Institutes of Health grant R21-DA017895-01, the Human Frontier Science Program, Young Investigator Awards from the Beckman Foundation and the Office of Naval Research, and a Klingenstein Fellowship in the Neurosciences. AD Mehta is a Rett Syndrome Research Foundation Fellow of the Life Sciences Research Foundation. BA Flusberg is funded by a National Science Foundation Graduate Research Fellowship.

References and recommended reading

Papers of particular interest, published within the annual period of review, have been highlighted as:

• of special interest

•• of outstanding interest

1. Yariv, A. Optical Electronics. edn 4. Sedra, AS., editor. Philadelphia: Saunders College Publishing; 1991.
2. Denk W, Svoboda K. Photon upmanship: why multiphoton imaging is more than a gimmick. Neuron 1997;18:351–357. [PubMed: 9115730]
3. Oheim M, Beaurepaire E, Chaigneau E, Mertz J, Charpak S. Two-photon microscopy in brain tissue: parameters influencing the imaging depth. J Neurosci Methods 2001;111:29–37. [PubMed: 11574117]
4. Jung JC, Schnitzer MJ. Multiphoton endoscopy. Opt Lett 2003;28:902–904. [PubMed: 12816240] This study introduced 2PFME using compound GRIN micro-lenses. The authors present triplet combinations of GRIN micro-lenses that are 350–1000 μm in diameter. Micron-scale resolution and the ability to visualize neurons and dendrites using 2PFME are demonstrated.
5. Jung JC, Mehta AD, Aksay E, Stepnoski R, Schnitzer MJ. *In vivo* mammalian brain imaging using one- and two-photon fluorescence microendoscopy. J Neurophysiol 2004;92 published online, DOI: 1001152/jn.00234.2004. The authors introduce one-photon epi-fluorescence microendoscopy employing doublet GRIN micro-lenses that are 350–1000 μm in diameter and provide micron-scale resolution. Using this technique, the authors obtain video-rate movies of individual red blood cells flowing through capillaries within hippocampal and thalamic areas of live rodents. Clusters of individual pyramidal neurons that express yellow fluorescent protein are visualized using one-photon microendoscopy in the CA1 hippocampal area of live transgenic mice. Along with the study of Levene *et al*. [6••], this paper also describes the initial *in vivo* usages of two-photon microendoscopy. Doublet GRIN microendoscopes positioned dorsal to the CA1 alveus are used to visualize individual fluorescent hippocampal pyramidal neurons and dendrites up to ~270 μm from the tip of the endoscope probe in live mice.
6. Levene MJ, Dombeck DA, Kasischke KA, Molloy RP, Webb WW. *In vivo* multiphoton microscopy of deep brain tissue. J Neurophysiol 2004;91:1908–1912. [PubMed: 14668300] Along with the work of Jung *et al*. [5••], this study describes the initial *in vivo* usages of two-photon microendoscopy. GRIN microendoscopes of the 350-μm-diameter triplet design [4•] are used to perform fast line-scan tracking of red blood cell flow in deep neocortical vessels of anesthetized mice. Fluorescent layer V neocortical pyramidal neurons and their dendrites, as well as CA1 hippocampal neuropil, are visualized in live transgenic mice.
7. Perchant A, Le Goualher G, Genet M, Viellerobe B, Berier F. An integrated fibered confocal microscopy system for *in vivo* and *in situ* fluorescence imaging – Applications to endoscopy in small animal imaging. 2004 IEEE International Symposium on Biomedical Imaging. 2004
8. Bird D, Gu M. Two-photon fluorescence endoscopy with a micro-optic scanning head. Opt Lett 2003;28:1552–1554. [PubMed: 12956376]

9. Tatagiba M, Matthies C, Samii M. Microendoscopy of the internal auditory canal in vestibular schwannoma surgery. Neurosurgery 1996;38:737–740. [PubMed: 8692393]
10. Jacobi PC, Dietlein TS, Krieglstein GK. Microendoscopic trabecular surgery in glaucoma management. Ophthalmology 1999;106:538–544. [PubMed: 10080211]
11. Rouse AR, Gmitro AF. Multispectral imaging with a confocal microendoscope. Opt Lett 2000;25:1708–1710. [PubMed: 18066321]
12. Sabharwal YS, Rouse AR, Donaldson L, Hopkins MF, Gmitro AF. Slit-scanning confocal microendoscope for high-resolution *in vivo* imaging. Appl Opt 1999;38:7133–7144. [PubMed: 18324260]
13. Knittel J, Schnieder L, Buess G, Messerschmidt B, Possner T. Endoscope-compatible confocal microscope using a gradient index-lens system. Opt Commun 2001;188:267–273.
14. Fisher JA, Civillico EF, Contreras D, Yodh AG. *In vivo* fluorescence microscopy of neuronal activity in three dimensions by use of voltage-sensitive dyes. Opt Lett 2004;29:71–73. [PubMed: 14719664]
15. Reed WA, Yan MF, Schnitzer MJ. Gradient-index fiber-optic microprobes for minimally invasive *in vivo* low-coherence interferometry. Opt Lett 2002;27:1794–1796. [PubMed: 18033366]
16. Theer P, Hasan MT, Denk W. Two-photon imaging to a depth of 1000 microns in living brains by use of a Ti:Al2O3 regenerative amplifier. Opt Lett 2003;28:1022–1024. [PubMed: 12836766] The authors describe a means of visualizing individual fluorescent cells within 800–1000 μm of the brain surface without using fiber optic probes. A regenerative amplifier light source operating at a 200 kHz repetition rate is shown to extend the imaging depth of two-photon microscopy to nearly the entire neocortex of 3-week-old mice.
17. Beaurepaire E, Oheim M, Mertz J. Ultra-deep two-photon fluorescence excitation in turbid media. Opt Commun 2001;188:25–29.
18. Mizrahi A, Crowley JC, Shtoyerman E, Katz LC. High-resolution *in vivo* imaging of hippocampal dendrites and spines. J Neurosci 2004;24:3147–3151. [PubMed: 15056694] The authors describe a means of visualizing individual fluorescent cells, dendrites, and spines within the dorsal-most layer of CA1 hippocampus in live mice using a surgical approach to aspirate overlying neocortical matter. A water immersion microscope objective positioned at the aspiration site enables *in vivo* hippocampal imaging by two-photon microscopy, without the use of fiber optic probes.
19. Kleinfeld D, Mitra PP, Helmchen F, Denk W. Fluctuations and stimulus-induced changes in blood flow observed in individual capillaries in layers 2 through 4 of rat neocortex. Proc Natl Acad Sci USA 1998;95:15741–15746. [PubMed: 9861040]
20. Devor A, Dunn AK, Andermann ML, Ulbert I, Boas DA, Dale AM. Coupling of total hemoglobin concentration, oxygenation, and neural activity in rat somatosensory cortex. Neuron 2003;39:353–359. [PubMed: 12873390]
21. Shtoyerman E, Arieli A, Slovin H, Vanzetta I, Grinvald A. Long-term optical imaging and spectroscopy reveal mechanisms underlying the intrinsic signal and stability of cortical maps in V1 of behaving monkeys. J Neurosci 2000;20:8111–8121. [PubMed: 11050133]
22. Malonek D, Grinvald A. Interactions between electrical activity and cortical microcirculation revealed by imaging spectroscopy: implications for functional brain mapping. Science 1996;272:551–554. [PubMed: 8614805]
23. Vanzetta I, Grinvald A. Increased cortical oxidative metabolism due to sensory stimulation: implications for functional brain imaging. Science 1999;286:1555–1558. [PubMed: 10567261]
24. Mayevsky A, Chance B. Intracellular oxidation-reduction state measured *in situ* by a multichannel fiber-optic surface fluorometer. Science 1982;217:537–540. [PubMed: 7201167]
25. Kasischke KA, Vishwasrao HD, Fisher PJ, Zipfel WR, Webb WW. Neural activity triggers neuronal oxidative metabolism followed by astrocytic glycolysis. Science 2004;305:99–103. [PubMed: 15232110]
26. Reinert KC, Dunbar RL, Gao W, Chen G, Ebner TJ. Flavoprotein autofluorescence imaging of neuronal activation in the cerebellar cortex *in vivo*. J Neurophysiol 2004;92:199–211. [PubMed: 14985415]
27. Murakami H, Kamatani D, Hishida R, Takao T, Kudoh M, Kawaguchi T, Tanaka R, Shibuki K. Short-term plasticity visualized with flavoprotein autofluorescence in the somatosensory cortex of anaesthetized rats. Eur J Neurosci 2004;19:1352–1360. [PubMed: 15016093]

28. Malonek D, Dirnagl U, Lindauer U, Yamada K, Kanno I, Grinvald A. Vascular imprints of neuronal activity: relationships between the dynamics of cortical blood flow, oxygenation, and volume changes following sensory stimulation. Proc Natl Acad Sci USA 1997;94:14826–14831. [PubMed: 9405698]
29. Anderson RE, Meyer FB. *In vivo* fluorescent imaging of NADH redox state in brain. Methods Enzymol 2002;352:482–494. [PubMed: 12125373]
30. Villringer A, Chance B. Non-invasive optical spectroscopy and imaging of human brain function. Trends Neurosci 1997;20:435–442. [PubMed: 9347608]
31. Grinvald, A.; Shmuel, A.; Vanzetta, I.; Shtoyerman, E.; Shoham, D.; Arieli, A. Intrinsic signal imaging in the neocortex. In: Yuste, R.; Lanni, F.; Konnerth, A., editors. Imaging Neurons. Vol. 45. Cold Spring Harbor Laboratory Press; 2000. p. 1-45.17
32. Cohen LB. Changes in neuron structure during action potential propagation and synaptic transmission. Physiol Rev 1973;53:373–418. [PubMed: 4349816]
33. Stepnoski RA, LaPorta A, Raccuia-Behling F, Blonder GE, Slusher RE, Kleinfeld D. Noninvasive detection of changes in membrane potential in cultured neurons by light scattering. Proc Natl Acad Sci USA 1991;88:9382–9386. [PubMed: 1946349]
34. Boas DA, Gaudette T, Strangman G, Cheng X, Marota JJ, Mandeville JB. The accuracy of near infrared spectroscopy and imaging during focal changes in cerebral hemodynamics. Neuroimage 2001;13:76–90. [PubMed: 11133311]
35. Baird AA, Kagan J, Gaudette T, Walz KA, Hershlag N, Boas DA. Frontal lobe activation during object permanence: data from near-infrared spectroscopy. Neuroimage 2002;16:1120–1125. [PubMed: 12202098]
36. Strangman G, Culver JP, Thompson JH, Boas DA. A quantitative comparison of simultaneous BOLD fMRI and NIRS recordings during functional brain activation. Neuroimage 2002;17:719–731. [PubMed: 12377147]
37. Hintz SR, Benaron DA, Siegel AM, Zourabian A, Stevenson DK, Boas DA. Bedside functional imaging of the premature infant brain during passive motor activation. J Perinat Med 2001;29:335–343. [PubMed: 11565203]
38. Boas DA, Franceschini MA. Diffuse optical imaging of brain activation: approaches to optimizing image sensitivity, resolution, and accuracy. Neuroimage. 2004 in press.
39. Maki A, Yamashita Y, Ito Y, Watanabe E, Mayanagi Y, Koizumi H. Spatial and temporal analysis of human motor activity using noninvasive NIR topography. Med Phys 1995;22:1997–2005. [PubMed: 8746704]
40. Bluestone AY, Abdulaev G, Schmitz CH, Barbour RL, Hielscher AH. Three-dimensional optical tomography of hemodynamics in the human head. Opt Express 2001;9:272–286. [PubMed: 19421298]
41. Siegel AM, Culver JP, Mandeville JB, Boas DA. Temporal comparison of functional brain imaging with diffuse optical tomography and fMRI during rat forepaw stimulation. Phys Med Biol 2003;48:1391–1403. [PubMed: 12812454]
42. Huppert TJ, Hoge RD, Franceschini MA, Boas DA. A temporal comparison of simultaneously acquired BOLD fMRI and near infrared spectroscopy (NIRS) hemodynamic response functions. Neuroimage. 2004 in press. This study compares the time course of blood oxygen level dependent (BOLD) signals acquired by fMRI in human subjects with the changes in total, oxy-, and deoxy-hemoglobin blood content as assessed simultaneously by NIRS during a finger tapping task. Of the three hemodynamic variables studied optically, the evolution of deoxy-hemoglobin content most closely follows the BOLD time course.
43. Wolf M, Wolf U, Choi JH, Gupta R, Safonova LP, Paunescu LA, Michalos A, Gratton E. Functional frequency-domain near-infrared spectroscopy detects fast neuronal signal in the motor cortex. Neuroimage 2002;17:1868–1875. [PubMed: 12498761]
44. Gratton G, Fabiani M. Shedding light on brain function: the event-related optical signal. Trends Cogn Sci 2001;5:357–363. [PubMed: 11477005]
45. Franceschini MA, Boas DA. Noninvasive measurement of neuronal activity with near-infrared optical imaging. Neuroimage 2004;21:372–386. [PubMed: 14741675]

46. Tsujimoto S, Yamamoto T, Kawaguchi H, Koizumi H, Sawaguchi T. Prefrontal cortical activation associated with working memory in adults and preschool children: an event-related optical topography study. Cereb Cortex 2004;14:703–712. [PubMed: 15084489]
47. Taga G, Asakawa K, Maki A, Konishi Y, Koizumi H. Brain imaging in awake infants by near-infrared optical topography. Proc Natl Acad Sci USA 2003;100:10722–10727. [PubMed: 12960368]
48. Culver JP, Siegel AM, Stott JJ, Boas DA. Volumetric diffuse optical tomography of brain activity. Opt Lett 2003;28:2061–2063. [PubMed: 14587815] The authors describe three-dimensional imaging of brain activation using DOT in an anesthetized rat preparation during electrical stimulation to the forepaw. The millimeter-scale resolution achieved is superior to the separation between optical fibers within an assembly mounted on the scalp. Regions of brain activation as identified by DOT are similar to those identified by fMRI during forepaw stimulation.
49. Culver JP, Durduran T, Furuya D, Cheung C, Greenberg JH, Yodh AG. Diffuse optical tomography of cerebral blood flow, oxygenation, and metabolism in rat during focal ischemia. J Cereb Blood Flow Metab 2003;23:911–924. [PubMed: 12902835]
50. Boas DA, Chen K, Grebert CD, Franceschini MA. Improving the diffuse optical imaging spatial resolution of the cerebral hemodynamic response to brain activation in humans. Opt Lett 2004;29:1506–1508. [PubMed: 15259728]
51. Xu H, Dehghani H, Pogue BW, Springett R, Paulsen KD, Dunn JF. Near-infrared imaging in the small animal brain: optimization of fiber positions. J Biomed Opt 2003;8:102–110. [PubMed: 12542386]
52. Pogue BW, Paulsen KD. High-resolution near-infrared tomographic imaging simulations of the rat cranium by use of *a priori* magnetic resonance imaging structural information. Opt Lett 1998;23:1716–1718. [PubMed: 18091894]
53. Barnett AH, Culver JP, Sorensen AG, Dale AM, Boas DA. Robust inference of baseline optical properties of the human head with three-dimensional segmentation from magnetic resonance imaging. Appl Opt 2003;42:3095–3108. [PubMed: 12790461]
54. Schulz RB, Ripoll J, Ntziachristos V. Experimental fluorescence tomography of tissues with noncontact measurements. IEEE Trans Med Imaging 2004;23:492–500. [PubMed: 15084074]
55. Schulz RB, Ripoll J, Ntziachristos V. Noncontact optical tomography of turbid media. Opt Lett 2003;28:1701–1703. [PubMed: 13677542]
56. Corlu A, Durduran T, Choe R, Schweiger M, Hillman EM, Arridge SR, Yodh AG. Uniqueness and wavelength optimization in continuous-wave multispectral diffuse optical tomography. Opt Lett 2003;28:2339–2341. [PubMed: 14680175]
57. Li A, Zhang Q, Culver JP, Miller EL, Boas DA. Reconstructing chromosphere concentration images directly by continuous-wave diffuse optical tomography. Opt Lett 2004;29:256–258. [PubMed: 14759043]
58. Prince S, Kolehmainen V, Kaipo JP, Franceschini MA, Boas DA, Arridge SR. Time-series estimation of biological factors in optical diffusion tomography. Phys Med Biol 2003;48:1491–1504. [PubMed: 12817933]
59. Thrush E, Levi O, Ha W, Carey G, Cook LJ, Deich J, Smith SJ, Moerner WE, Harris JS Jr. Integrated semiconductor vertical-cavity surface-emitting lasers and PIN photodetectors for biomedical fluorescence sensing. IEEE J Quantum Electron 2004;40:491–498.
60. Huang D, Swanson EA, Lin CP, Schuman JS, Stinson WG, Chang W, Hee MR, Flotte T, Gregory K, Puliafito CA, et al. Optical coherence tomography. Science 1991;254:1178–1181. [PubMed: 1957169]
61. Fujimoto JG. Optical coherence tomography for ultrahigh resolution *in vivo* imaging. Nat Biotechnol 2003;21:1361–1367. [PubMed: 14595364]
62. Drexler W, Morgner U, Ghanta RK, Kärtner FX, Schuman JS, Fujimoto JG. Ultrahigh-resolution ophthalmic optical coherence tomography. Nat Med 2001;7:502–507. [PubMed: 11283681]
63. Drexler W. Ultrahigh-resolution optical coherence tomography. J Biomed Opt 2004;9:47–74. [PubMed: 14715057] The author describes in detail the use of novel broad bandwidth optical sources for ultrahigh-resolution OCT, with particular emphasis on *in vivo* imaging of the retina with micron-scale axial resolution in human subjects.

64. Unterhuber A, Povazay B, Bizheva K, Hermann B, Sattmann H, Stingl A, Le T, Seefeld M, Menzel R, Preusser M, et al. Advances in broad bandwidth light sources for ultrahigh resolution optical coherence tomography. Phys Med Biol 2004;49:1235–1246. [PubMed: 15128201]

65. Tearney GJ, Brezinski ME, Bouma BE, Boppart SA, Pitris C, Southern JF, Fujimoto JG. *In vivo* endoscopic optical biopsy with optical coherence tomography. Science 1997;276:2037–2039. [PubMed: 9197265]

66. Li X, Chudoba C, Ko T, Pitris C, Fujimoto JG. Imaging needle for optical coherence tomography. Opt Lett 2000;25:1520–1522. [PubMed: 18066265]

67. Herz PR, Chen Y, Aguirre AD, Schneider K, Hsiung P, Fujimoto JG, Madden K, Schmitt J, Goodnow J, Petersen C. Micro-motor endoscope catheter for *in vivo* ultrahigh resolution optical coherence tomography. Opt Lett. 2004 in press.

68. Tran PH, Mukai DS, Brenner M, Chen Z. *In vivo* endoscopic optical coherence tomography by use of a rotational microelectromechanical system probe. Opt Lett 2004;29:1236–1238. [PubMed: 15209258]

69. Boppart SA, Bouma BE, Pitris C, Southern JF, Brezinski ME, Fujimoto JG. *In vivo* cellular optical coherence tomography imaging. Nat Med 1998;4:861–865. [PubMed: 9662382]

70. Drexler W, Morgner U, Krtner FX, Pitris C, Boppart SA, Li XD, Ippen EP, Fujimoto JG. *In vivo* ultrahigh-resolution optical coherence tomography. Opt Lett 1999;24:1221–1223. [PubMed: 18073990]

71. Morgner U, Drexler W, Krtner FX, Li XD, Pitris C, Ippen EP, Fujimoto JG. Spectroscopic optical coherence tomography. Opt Lett 2000;25:111–113. [PubMed: 18059799]

72. de Boer JF, Cense B, Park BH, Pierce MC, Tearney GJ, Bouma BE. Improved signal-to-noise ratio in spectral-domain compared with time-domain optical coherence tomography. Opt Lett 2003;28:2067–2069. [PubMed: 14587817] This study and that by Leitgeb *et al*. [74•] compare the sensitivity of OCT using spectral-domain detection to that using time-domain detection. Spectral-domain OCT is shown to be up to several hundred times more sensitive.

73. Fercher AF, Hitzenberger CK, Kamp G, El-Zaiat SY. Measurement of intraocular distances by backscattering spectral interferometry. Opt Commun 1995;117:43–48.

74. Leitgeb R, Hitzenberger CK, Fercher AF. Performance of fourier domain vs. time domain optical coherence tomography. Opt Express 2003;11:889–894. [PubMed: 19461802] This study and that by de Boer *et al*. [72•] compare the sensitivity of OCT using fourier-domain detection versus time-domain detection. Fourier-domain OCT is shown to be significantly more sensitive.

75. Nassif N, Cense B, Park BH, Yun SH, Chen TC, Bouma BE, Tearney GJ, de Boer JF. *In vivo* human retinal imaging by ultrahigh-speed spectral domain optical coherence tomography. Opt Lett 2004;29:480–482. [PubMed: 15005199]

76. Wojtkowski M, Bajraszewski T, Targowski P, Kowalczyk A. Real-time *in vivo* imaging by high-speed spectral optical coherence tomography. Opt Lett 2003;28:1745–1747. [PubMed: 14514087]

77. Nassif N, Cense B, Park BH, Pierce MC, Yun SH, Bouma BE, Tearney GJ, Chen TC, de Boer JF. *In vivo* high-resolution video-rate spectral domain optical coherence tomography of the human retina and optic nerve. Opt Express 2004;12:367–376. [PubMed: 19474832]

78. White BR, Pierce MC, Nassif N, Cense B, Park BH, Tearney GJ, Bouma BE, Chen TC, de Boer JF. *In vivo* dynamic human retinal blood flow imaging using ultra-high-speed spectral domain optical Doppler tomography. Opt Express 2003;11:3490–3497. [PubMed: 19471483] The authors demonstrate video-rate imaging of retinal blood flow using spectral-domain OCT. Analysis of the optical Doppler shifts that arise from blood movement allow arterial, venous, and even capillary flow to be identified. The especially pulsatile character of retinal arterial flow can be seen within video-rate movies.

79. Leitgeb RA, Schmetterer L, Drexler W, Fercher AF, Zawadzki RJ, Bajraszewski T. Real-time assessment of retinal blood flow with ultrafast acquisition by color Doppler Fourier domain optical coherence tomography. Opt Express 2003;11:3116–3121. [PubMed: 19471434]

80. Cense B, Nassif N, Chen TC, Pierce MC, Yun SH, Park BH, Bouma BE, Tearney GJ, de Boer JF. Ultrahigh-resolution high-speed retinal imaging using spectral-domain optical coherence tomography. Opt Express 2004;12:2435–2447. [PubMed: 19475080]

81. Wojtkowski M, Srinivasan VJ, Ko TH, Fujimoto JG, Kowalczyk A, Duker JS. Ultrahigh-resolution, high-speed, Fourier domain optical coherence tomography and methods for dispersion compensation. Opt Express 2004;12:2404–2422. [PubMed: 19475077]
82. Leitgeb RA, Drexler W, Unterhuber A, Hermann B, Bajraszewski T, Le T, Stingl A, Fercher AF. Ultrahigh resolution Fourier domain optical coherence tomography. Opt Express 2004;12:2156–2165. [PubMed: 19475051]
83. Yun SH, Tearney GJ, de Boer JF, Iftimia N, Bouma BE. High-speed optical frequency-domain imaging. Opt Express 2003;11:2953–2963. [PubMed: 19471415]
84. Choma MA, Sarunic MV, Yang C, Izatt JA. Sensitivity advantage of swept source and Fourier domain optical coherence tomography. Opt Express 2003;11:2183–2189. [PubMed: 19466106]
85. Maheswari RU, Takaoka H, Kadono H, Homma R, Tanifuji M. Novel functional imaging technique from brain surface with optical coherence tomography enabling visualization of depth resolved functional structure *in vivo*. J Neurosci Methods 2003;124:83–92. [PubMed: 12648767] The authors describe the first usage of *in vivo* fOCT for detecting slow intrinsic optical signals indicative of brain activation. Studies of visual cortex in anesthetized cats revealed sensory-evoked intrinsic signals that varied with cortical depth.
86. Bizheva K, Unterhuber A, Hermann B, Povazay B, Sattmann H, Drexler W, Stingl A, Le T, Mei M, Holzwarth R, et al. Imaging *ex vivo* and *in vitro* brain morphology in animal models with ultrahigh resolution optical coherence tomography. J Biomed Opt 2004;9:719–724. [PubMed: 15250758]
87. Iftimia N, Bouma BE, Tearney GJ. Speckle reduction in optical coherence tomography by “path length encoded” angular compounding. J Biomed Opt 2003;8:260–263. [PubMed: 12683852]
88. Boppart SA, Brezinski ME, Pitris C, Fujimoto JG. Optical coherence tomography for neurosurgical imaging of human intracortical melanoma. Neurosurgery 1998;43:834–841. [PubMed: 9766311]
89. Lazebnik M, Marks DL, Potgieter K, Gillette R, Boppart SA. Functional optical coherence tomography for detecting neural activity through scattering changes. Opt Lett 2003;28:1218–1220. [PubMed: 12885026]
90. Akkin T, Dave DP, Milner TE, Rylander HG III. Detection of neural activity using phase-sensitive optical low-coherence relfectometry. Opt Express 2004;12:2377–2386. [PubMed: 19475074] The authors use a differential phase-sensitive version of LCI to detect fast axonal movements of <1 nm accompanying electrically stimulated action potentials in an *in vitro* preparation of crayfish leg nerve bundles. To reveal these fine displacements, the authors averaged over hundreds of stimulation trials. The displacements appear to be nearly simultaneous with action potential occurrence to within ~1 ms.
91. Kholodnykh AI, Petrova IY, Larin KV, Motamedi M, Esenaliev RO. Precision of measurement of tissue optical properties with optical coherence tomography. Appl Opt 2003;42:3027–3037. [PubMed: 12790454]
92. Pircher M, Gotzinger E, Leitgeb R, Fercher AF, Hitzenberger CK. Speckle reduction in optical coherence tomography by frequency compounding. J Biomed Opt 2003;8:565–569. [PubMed: 12880365]
93. Lee TM, Oldenburg AL, Sitafalwalla S, Marks DL, Luo W, Toublan FJ, Suslick KS, Boppart SA. Engineered microsphere contrast agents for optical coherence tomography. Opt Lett 2003;28:1546–1548. [PubMed: 12956374]
94. Rao KD, Choma MA, Yazdanfar S, Rollins AM, Izatt JA. Molecular contrast in optical coherence tomography by use of a pump-probe technique. Opt Lett 2003;28:340–342. [PubMed: 12659437] This study and those by Yang *et al*. and Xu *et al*. [95•,96•] introduce the use of molecular imaging contrast agents for OCT.
95. Yang C, Choma MA, Lamb LE, Simon JD, Izatt JA. Protein-based molecular contrast optical coherence tomography with phytochrome as the contrast agent. Opt Lett 2004;29:1396–1398. [PubMed: 15233447] This study and those by Rao *et al*. and Xu *et al*. [94•,96•] introduce the use of molecular imaging contrast agents for OCT.
96. Xu C, Ye J, Marks DL, Boppart SA. Near-infrared dyes as contrast-enhancing agents for spectroscopic optical coherence tomography. Opt Lett 2004;29:1647–1649. [PubMed: 15309847] This study and those by Rao *et al*. and Yang *et al*. [94•,95•] introduce the use of molecular imaging contrast agents for OCT.

97. Faber DJ, Mik EG, Aalders MCG, van Leeuwen TG. Light absorption of (oxy-)hemoglobin assessed by spectroscopic optical coherence tomography. Opt Lett 2003;28:1436–1438. [PubMed: 12943083]
98. Unterhuber A, Povazay B, Hermann B, Sattmann H, Drexler W, Yakovlev V, Tempea G, Schubert C, Anger EM, Ahnelt PK, et al. Compact, low-cost Ti:Al2O3 laser for *in vivo* ultrahigh-resolution optical coherence tomography. Opt Lett 2003;28:905–907. [PubMed: 12816241]
99. Povazay B, Bizheva K, Unterhuber A, Hermann B, Sattmann H, Fercher AF, Drexler W, Apolonski A, Wadsworth WJ, Knight JC, et al. Submicrometer axial resolution optical coherence tomography. Opt Lett 2002;27:1800–1802. [PubMed: 18033368]
100. Bourquin S, Aguirre AD, Hartl I, Hsiung P, Ko TH, Fujimoto JG, Birks TA, Wadsworth WJ, Bunting U, Kopf D. Ultrahigh resolution real time OCT imaging using a compact femtosecond Nd: Glass laser and nonlinear fiber. Opt Express 2003;11:3290–3297. [PubMed: 19471457]
101. Ko TH, Adler DC, Fujimoto JG, Mamedov D, Prokhorov V, Shidlovski V, Yakubovich S. Ultrahigh resolution optical coherence tomography imaging with a broadband superluminescent diode light source. Opt Express 2004;12:2112–2119. [PubMed: 19475046]
102. Yun SH, Boudoux C, Tearney GJ, Bouma BE. High-speed wavelength-swept semiconductor laser with a polygon-scanner-based wavelength filter. Opt Lett 2003;28:1981–1983. [PubMed: 14587796]
103. Vinegoni C, Bredfeldt JS, Marks DL, Boppart SA. Nonlinear optical contrast enhancement for optical coherence tomography. Opt Express 2004;12:331–341. [PubMed: 19471542]
104. Jiang Y, Tomov I, Wang Y, Chen Z. Second-harmonic optical coherence tomography. Opt Lett 2004;29:1090–1092. [PubMed: 15181995]
105. Martin C, Berwick J, Johnston D, Zheng Y, Martindale J, Port M, Redgrave P, Mayhew J. Optical imaging spectroscopy in the unanaesthetised rat. J Neurosci Methods 2002;120:25–34. [PubMed: 12351204]
106. Berwick J, Martin C, Martindale J, Jones M, Johnston D, Zheng Y, Redgrave P, Mayhew J. Hemodynamic response in the unanesthetized rat: intrinsic optical imaging and spectroscopy of the barrel cortex. J Cereb Blood Flow Metab 2002;22:670–679. [PubMed: 12045665]
107. Vanzetta I, Slovin H, Omer DB, Grinvald A. Columnar resolution of blood volume and oximetry functional maps in the behaving monkey; implications for FMRI. Neuron 2004;42:843–854. [PubMed: 15182722]
108. Rector D, Harper R. Imaging of hippocampal neural activity in freely behaving animals. Behav Brain Res 1991;42:143–149. [PubMed: 2059328]
109. Poe GR, Rector DM, Harper RM. Hippocampal reflected optical patterns during sleep and waking states in the freely behaving cat. J Neurosci 1994;14:2933–2942. [PubMed: 8182449]
110. Poe GR, Kristensen MP, Rector DM, Harper RM. Hippocampal activity during transient respiratory events in the freely behaving cat. Neuroscience 1996;72:39–48. [PubMed: 8730704]
111. Helmchen F, Fee MS, Tank DW, Denk W. A miniature head-mounted two-photon microscope: high-resolution brain imaging in freely moving animals. Neuron 2001;31:903–912. [PubMed: 11580892]
112. Dickensheets, D.; Kino, GS. A scanned optical fiber confocal microscope. In: Cogswell, CJ.; Carlsson, K., editors. SPIE Symposium on Electronic Imaging Science & Technology; San Jose, CA. Society of Photo-Optical Instrumentation Engineers; 1994. p. 39-47.
113. Gobel W, Nimmerjahn A, Helmchen F. Distortion-free delivery of nanjoule femtosecond pulses from a Ti:sapphire laser through a hollow-core photonic crystal fiber. Opt Lett 2004;29:1285–1287. [PubMed: 15209273]
114. Nimmerjahn, A.; Denk, W.; Helmchen, F. Two-photon fiberscope imaging of cellular networks in the neocortex *in vivo*; Society for Neuroscience Annual Meeting; 2003. Program No. 218.16
115. Dickensheets DL, Kino GS. Micromachined scanning confocal optical microscope. Opt Lett 1996;21:764–766. [PubMed: 19876151]
116. Kwon S, Lee LP. Micromachined transmissive scanning confocal microscope. Opt Lett 2004;29:706–708. [PubMed: 15072365]
117. Zara JM, Yazdanfar S, Rao KD, Izatt JA, Smith SW. Electrostatic micromachine scanning mirror for optical coherence tomography. Opt Lett 2003;28:628–630. [PubMed: 12703922]

118. Piyawattanametha, W.; Fan, L.; Hsu, S.; Fujino, M.; Wu, MC.; Herz, PR.; Aguirre, AD.; Chen, Y.; Fujimoto, JG. Two-dimensional endoscopic MEMS scanner for high-resolution optical coherence tomography; Conference on Lasers and Electro-Optics; 2004. Program No. CWS 2

119. Xie T, Xie H, Fedder GK, Pan Y. Endoscopic optical coherence tomography with a modified microelectromechanical systems mirror for detection of bladder cancers. Appl Opt 2003;42:6422–6426. [PubMed: 14649286]

120. Anger EM, Unterhuber A, Hermann B, Sattmann H, Schubert C, Morgan JE, Cowey A, Ahnelt PK, Drexler W. Ultrahigh resolution optical coherence tomography of the monkey fovea. Identification of retinal sublayers by correlation with semithin histology sections. Exp Eye Res 2004;78:1117–1125. [PubMed: 15109918]

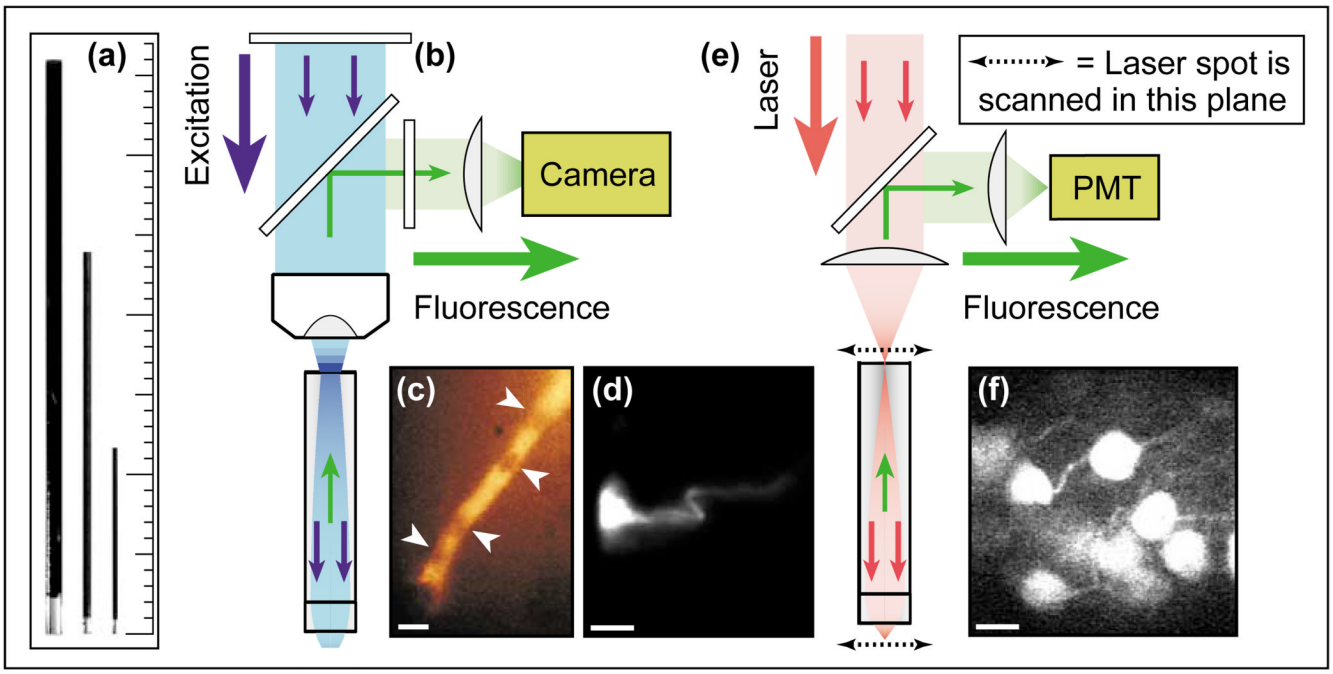

Figure 1.

Fluorescence microendoscopy (FME). **(a)** Doublet microendoscope probes, 1000 μm, 500 μm, and 350 μm in diameter. Each probe comprises two GRIN micro-lenses, an endoscopic objective lens and a relay lens. The objective lenses are oriented down, and the relay lenses exhibit a dark coating. The minor tick on the scale is 1 mm. **(b)** Optical schematic of one-photon FME. Fluorescence excitation light (blue) passes through a filter and dichroic mirror, and is coupled into the doublet microendoscope probe using a conventional microscope objective. The probe delivers the excitation light to the specimen, and fluorescence emissions (green) return back through the probe, the microscope objective lens, and an emission filter. The fluorescence image can be viewed through eyepieces or projected onto a camera. **(c)** Individual frame of a video-rate movie acquired by one-photon FME of red blood cells passing single-file through a capillary in the laterodorsal thalamus of an anesthetized rat. White arrowheads point to individual red blood cells. **(d)** One-photon FME image of a neuron labeled with the fluorescent dye Di-I in the somatosensory neocortex of an anesthetized rat. **(e)** Optical schematic of two-photon fluorescence microendoscopy (2PFME) [4•,5••,6••]. An ultra-short pulsed laser beam is focused just external to the relay lens of the microendoscope probe. The focal spot is raster scanned in two lateral dimensions, and the probe projects and demagnifies the scan pattern to the specimen plane. Two-photon excited fluorescence originates from the laser focus in the specimen, returns through the endoscope probe, is separated from the laser light, and is detected by a photomultiplier tube (PMT). A computer controls the scanning process and constructs the digital image. **(f)** Image of multiple CA1 hippocampal pyramidal cell bodies acquired by 2PFME in an anesthetized mouse engineered to express the yellow fluorescent protein in a subset of these neurons. The scale bars in panels (c), (d), and (f) are 10 μm. This figure is based on material from references [4•,5••].

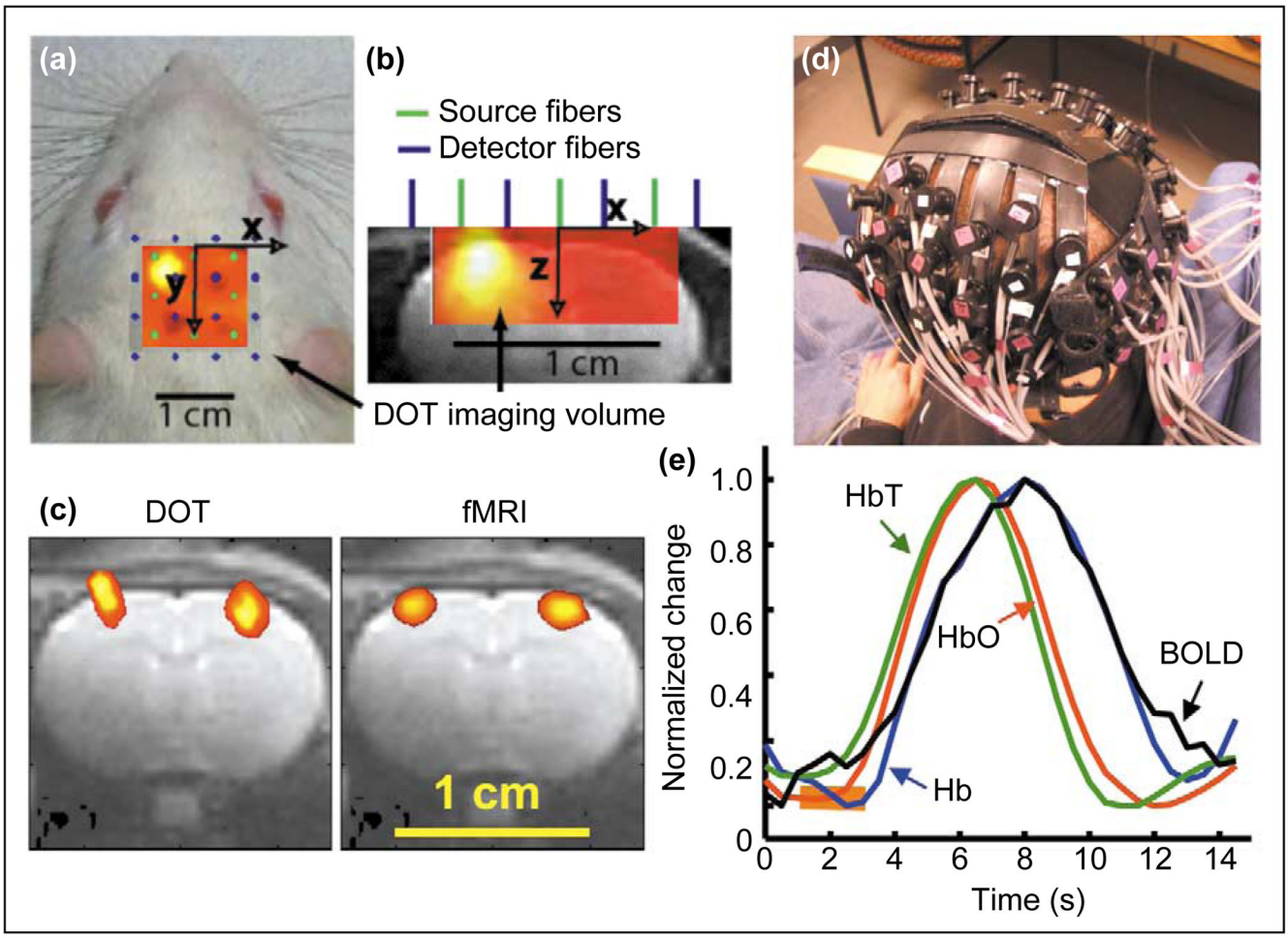

Figure 2.

Diffuse optical imaging (DOI) and tomography (DOT). (a–c) DOT in an anesthetized rat preparation. **(a)** Locations of 9 source (green dots) and 16 detector (blue dots) 100-μm-diameter optical fibers placed on the scalp dorsal to the somatosensory cortex of an anesthetized rat. Each source fiber emitted light from a pair of laser diodes with wavelengths of 690 and 830 nm. Each of the 18 laser diodes was intensity modulated in a square wave at a unique frequency between 4 and 8 kHz, allowing the signals from distinct light sources to be distinguished at each detector. The forepaw of the rat was stimulated electrically using 200 μs pulses of 1.0 mA current repeating at 3 Hz for 6 s duration, with 54 s between stimulus presentations. The pattern of activation, as assessed using the change in absorbance at 830 nm averaged over 32 stimulus presentations, is superimposed on the fiber array and the image of the rat, with warmer colors indicating greater magnitude of activation. **(b)** A transverse view of the rat cerebrum and fiber configuration, with the pattern of brain activation in response to forepaw stimulation superimposed on an anatomical image obtained by MRI. **(c)** A comparison of the brain regions that are activated by left and right forepaw stimulation as identified by DOT versus those identified by functional magnetic resonance imaging (fMRI) using the same stimulation protocol and a superparamagnetic contrast agent, monocrystalline iron oxide nanoparticles (MION), for detecting changes in cerebral blood volume. Although there is good agreement regarding the lateral separation of the two identified regions, the activated regions found by DOT are larger than those found by fMRI and also extend into the scalp and skull. The latter effect is a common artifact with DOT that occurs when image reconstruction is performed

without mathematically constraining absorbance changes to the brain. Areas of activation are then biased somewhat towards the scalp. (d and e) DOI in human subjects. **(d)** An assembly of optical fibers worn on the head of a human subject for DOI. (e) A comparison between the total (green curve), oxy- (red curve), and deoxy-hemoglobin (blue curve) content as determined by DOI and the blood oxygen level-dependent (BOLD) signal (black curve) as measured by fMRI, in a human subject who performed finger tapping for 2 s (orange bar). Each curve is an average of 27 trials. The material in this figure was provided by DA Boas of Massachusetts General Hospital. Panels (a–c) are based on material from references [41,48••], panels (d,e) are based on material from reference [42•].

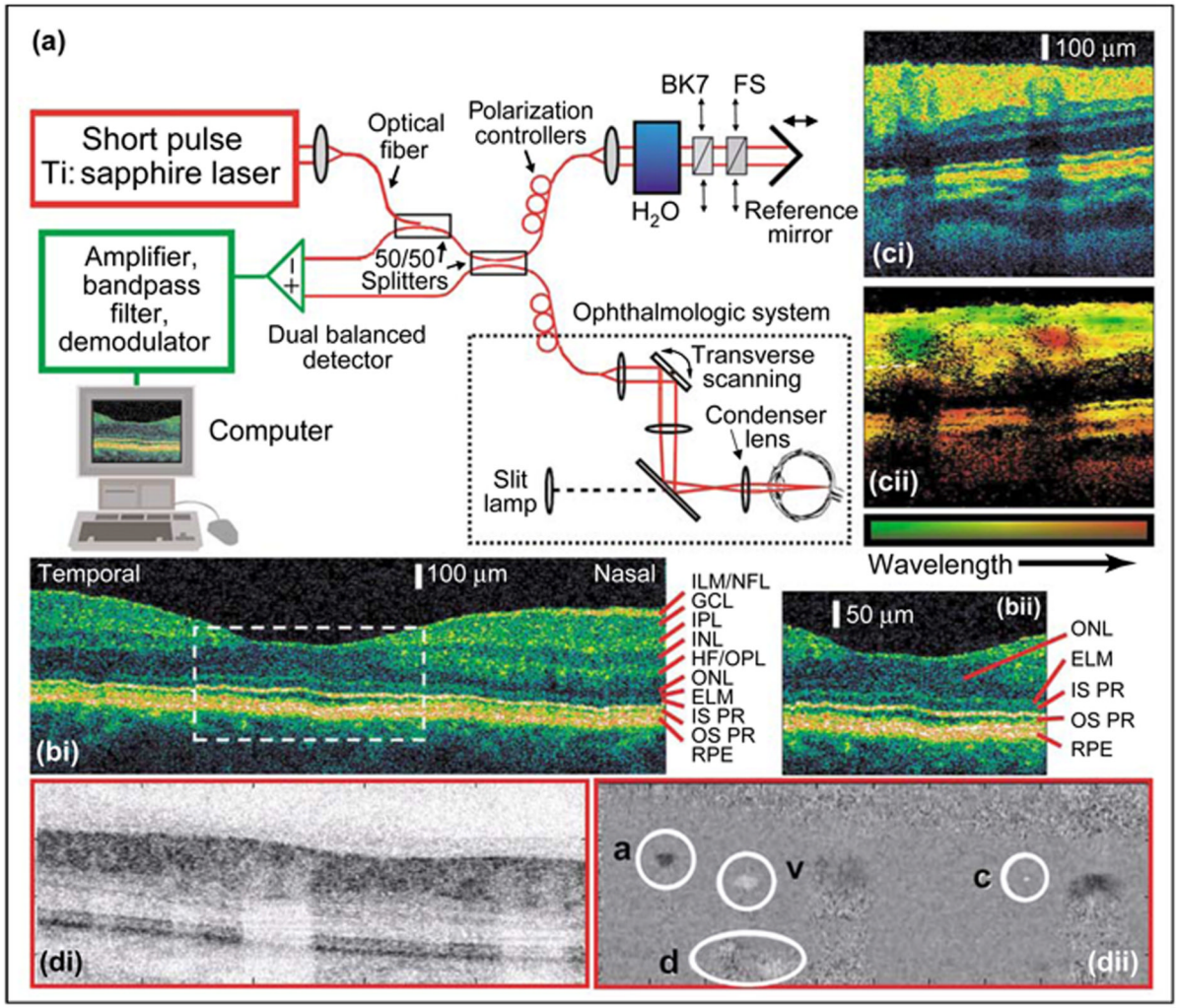

Figure 3.

Ultrahigh-resolution *in vivo* optical coherence tomography (OCT) of the human retina. **(a)** Optical schematic of ultrahigh-resolution OCT. The main optical paths are shown in red, electronic components in green. A Titanium:sapphire laser emits pulses of under 10 fs duration with a spectrum centered at 800 nm and a bandwidth of ~165 nm full width at half maximum. This bandwidth yields a coherence length of ~2 µm in air, ~1.4 µm in tissue, and sets the optimal axial resolution of optical sectioning. The laser light is coupled into a fiber optic Michelson interferometer in which the sample arm comprises the ophthalmologic system. Using broad bandwidth fiber optic 50/50 splitters, nearly equal intensities of light are directed into the interferometer reference and sample arms. In the reference arm the light is coupled from optical fiber into free space, reflects off a translating reference mirror, and returns into the optical fiber. The position of the translating mirror sets the optical path length of the reference arm. Light in the sample arm that travels an equivalent optical path length, to within a coherence length, recombines interferometrically with light in the reference arm. The amplitude of this interferometric signal represents the contrast parameter in conventional OCT. Scanning the position of the reference mirror varies the depth of the optical section acquired within retinal tissue, and the scanning speed sets the Doppler frequency shift of light in the reference arm. This Doppler frequency becomes the heterodyne detection frequency from which the interferometric amplitude is extracted. In the sample arm, the subject sits at an

ophthalmic slit lamp, and a lens system focuses laser light that has been coupled into free space onto the subject's retina. The resulting weak focal spot, about ~15 μm at the waist, is scanned in a transverse direction across the retina. A fraction of the light focused onto the retina backscatters and re-enters the interferometer. To optimize the interferometric signal, fiber optic polarization controllers in both the sample and reference arms are adjusted to match the polarization of light within the two arms. Chromatic dispersion must also be matched, or else optical sectioning degrades. To balance dispersion occurring within ~25 mm of ocular media, light in the reference arm travels through 25 mm of water. Chromatic dispersion is fine-tuned using two translatable prism pairs, one of fused silica (FS), the other BK7 high-index glass (BK7), which allow the thickness of glass in the reference arm to be varied. The interferometer design includes two 50/50 splitters that enable dual balanced detection. This detection approach cancels amplitude fluctuations common to the two arms, such as laser power noise, and increases the detection sensitivity to nearly the physical limit set by photon shot noise. An amplified version of the interferometer signal is band-pass filtered around the Doppler frequency of the reference arm and then demodulated. A computer reconstructs the retinal tomogram. Because the dynamic range of backscattering signals from tissue typically extends over several orders of magnitude, OCT images are usually represented on a logarithmic scale. **(b)** *In vivo* OCT retinal tomogram of the foveal region of a normal human subject. **(i)** Comparisons between OCT retinal images and excised retinal tissue have led to histological assignments as indicated by the red lines [62,120]. Abbreviations: ELM, external limiting membrane; GCL, ganglion cell layer; HF, Henle's fiber layer; ILM, internal limiting membrane; INL, inner nuclear layer; IPL, inner plexiform layer; IS PR, inner segment of photoreceptor layer; NFL, nerve fiber layer; ONL, outer nuclear layer; OPL, outer plexiform layer; OS PR, outer segment of photoreceptor layer; RPE, retinal pigment epithelium. **(ii)** An enlarged view of the foveal area enclosed by the white dashed lines in panel (bi). Panel **(c)** shows a comparison between conventional and spectroscopic OCT retinal imaging. **(i)** An *in vivo* OCT human retinal tomogram. **(ii)** A spectroscopic OCT tomogram of the same retinal area as in panel (ci). The mean wavelength of backscattered light is encoded by the color hue, with shorter wavelengths assigned to greener hues and longer wavelengths to redder hues, as indicated by the color bar. The intensity of backscattered light is encoded by the color saturation. A vein shown in green and an artery shown in red that are not easily identifiable by conventional OCT are apparent in the spectroscopic OCT image. The blood vessels attenuate light and so the underlying areas appear darkened in (ci and cii). This illustrates the confound between attenuation and backscattering that can arise in OCT image interpretation. The two vessels backscatter light of different spectra, in part because their opposing directions of blood flow induce Doppler frequency shifts of opposite sign. The distinct absorption spectra of oxy- and deoxy-hemoglobin across the laser emission band are additional influences. Oxy-hemoglobin has the higher extinction coefficient for wavelengths above ~800 nm, the hemoglobin isobestic point. Deoxy-hemoglobin has the higher extinction coefficient below ~800 nm. This difference helps the artery and vein to be distinguished on the basis of the wavelength dependence of signal attenuation in the respective underlying tissues. **(d)** *In vivo* spectral- or Fourier-domain OCT of the human retina and retinal blood flow. Using multiple spectral detection channels, rather than temporal domain detection as shown in (a), Fourier-domain OCT eliminates the need for scanning the path length of the reference arm and improves sensitivity by eliminating common shot noise between distinct spectral channels [72•,75–77, 78••,79–82]. This increased sensitivity can be harnessed to perform ultrahigh-speed imaging, and panel **(i)** shows a single frame from a video-rate movie of the human retina. As in (c), shadowing beneath blood vessels is evident. **(ii)** An OCT phase or Doppler image of the same retinal region as in (di), also acquired using spectral detection. The Doppler image is constructed by extracting the phase difference in the OCT signal between points at the same optical path length in adjacent lines of the image. This phase difference encodes the bi-directional Doppler frequency shift induced by moving particles and is encoded on a gray-scale from +12 kHz (black) to −12 kHz (white), where gray indicates no Doppler shift. Locations

of an artery (a), vein (v), capillary (c), and deep blood flow (d) within the retinal choroid are circled. The video-rate Doppler movie from which this frame was taken reveals pulsatile blood flow within the artery and less variable flow in the opposite direction within the vein. The capillary is slightly under 10 μm in diameter. The material in panels (a–c) was supplied by W Drexler of the University of Vienna and is based on material from references [62,63•]. The material in panel (d) was provided by JF de Boer, GJ Tearney, and BE Bouma of Massachusetts General Hospital and is based on material from reference [78••].

Table 1

A comparison of fluorescence and intrinsic signal based fiber optic mammalian brain imaging modalities.

Imaging Modality	Usage	Typical probe dimensions	Advantages	Limitations
Fluorescence modalities				
One-photon fluorescence microendoscopy [5••]	Camera-based imaging deep within tissue	350–1000 μm diameter	Full-frame acquisition, cellular resolution deep within tissue, ease of use, and low cost.	Mechanical insertion of probe may disrupt tissue. Does not reject out of focus fluorescence. Typical field of view is about 60–250 μm in diameter.
Two-photon fluorescence microendoscopy [4•,5••,8]	Laser-scanning imaging deep within tissue	350–1000 μm diameter	Inherent optical sectioning, cellular resolution deep within tissue, and optical penetration depths of up to hundreds of microns from the tip of the endoscope.	Mechanical insertion of probe may disrupt tissue. Typical field of view is about 60–250 μm in diameter.
Confocal microendoscopy [7,11–13]	Commonly employs a fiber bundle, applications under development	1–8 mm diameter	Cellular resolution, mechanical flexibility, ease of use, and optical sectioning.	Optical penetration depth only ~25–50 μm. Often lacks built-in focal control. Use of fiber bundles can degrade resolution to ~2–5 μm. Field of view of ~250–1000 μm in diameter.
Miniature two-photon microscopy [111,114]	Secured on cranium, scanning fiber mechanism	11–25 g, ~1.3 cm diameter	Allows cellular imaging in freely moving animals, inherent optical sectioning, and imaging depths of up to ~250 μm below the brain surface.	Images subject to motion artifact. Devices currently too big for use in mice. Field of view is up to a few hundred microns across.
Fluorescence endoscopy [14,24]	Camera-based imaging secured on cranium	Around 2 mm diameter	Can access intrinsic fluorescence signals or neuronal population activity	Lacks true optical sectioning and cannot resolve cells.

Imaging Modality	Usage	Typical probe dimensions	Advantages	Limitations
			using voltage-sensitive dyes. Field of view ~2 mm across.	
Intrinsic signal modalities				
Diffuse optical imaging using near infrared spectroscopy [34–36,105]	Assembly of optical fibers on scalp	Fiber assemblies can extend over large portions of the head.	Provides topographic maps of brain activity. Distinguishes changes in total, oxy-, and deoxy-hemoglobin blood content. Portable low cost fiber assembly can be used in subjects who are freely moving or who cannot undergo MRI.	Centimeter-scale resolution in humans. Poorer spatial resolution than DOT. Poor penetration depth into human cortex. Sensitive to physiological noise artifacts.
Diffuse optical tomography [34,40,41,48••,49,56]	Assembly of optical fibers on scalp	Fiber assemblies can extend over large portions of the head.	Portable volumetric imaging of brain activity at low cost. Distinguishes changes in total, oxy- and deoxy-hemoglobin blood content. Resolution superior to the distance between fibers. Can be used in subjects who are freely moving or who cannot undergo MRI.	Poorer spatial resolution and penetration depth into human cortex than fMRI. Spatial resolution declines with tissue depth below scalp. Sensitive to physiological noise artifacts.
Optical coherence tomography [60–63,75,77,79,82]	Light from a single fiber is scanned over sample	Varies widely. Both miniature probes and free-standing instruments exist.	Optical sectioning, 90–110 dB typical sensitivity, micron-scale resolution. Video-rate retinal imaging and blood flow imaging in individual vessels achieved.	Image contrast can be difficult to interpret, speckle noise power is proportional to signal power and is usually larger than neural activity-related optical signals.
Miniature endoscopy [105,109,110]	Camera-based imaging secured on cranium	As small as 1.5–2 mm in diameter	Images optical signatures of metabolic responses to brain activity. Has been used in	Lacks optical sectioning, image quality and spatial resolution has often been

Imaging Modality	Usage	Typical probe dimensions	Advantages	Limitations
			restrained alert rats and freely moving cats.	poor. Typically lacks built-in focal control.